OXFORD UNIVERSITY PRESS | American Journal Of Epidemiology

Radio-biologically Motivated Modeling of Radiation Risks of Mortality From Ischemic Heart Diseases in the Canadian Fluoroscopy Cohort Study

Journal:	*American Journal of Epidemiology*
Manuscript ID	Draft
Manuscript Type:	Original Contribution
Key Words:	ischemic heart diseases, ionizing radiation, multi-model inference, dose-response, nonlinear

Title: Radio-biologically Motivated Modeling of Radiation Risks of Mortality From Ischemic Heart Diseases in the Canadian Fluoroscopy Cohort Study

Abbreviations: CFCS, Canadian Fluoroscopy Cohort Study; CI, confidence interval; CVD, cardiovascular disease; *ERR*, excess relative risk; HMGU, Helmholtz Zentrum München; ICD-9, International Classification of Diseases and Causes of Death, Ninth Revision; LRT, likelihood ratio test; IHD, ischemic heart diseases; IR, ionizing radiation; LNT model, linear no-threshold model; LTH model, linear threshold model; LSS, Life Span Study; MLE, maximum likelihood estimate; MMI, multi-model inference.

Running head: Radio-biological modeling of IHD risks

ABSTRACT

Recent analyses of the Canadian Fluoroscopy Cohort Study reported significantly increased radiation risks of mortality from ischemic heart diseases (IHD) with a linear dose-response adjusted for dose fractionation. This cohort incudes 63,707 tuberculosis patients from Canada who were exposed to low-to-moderate-dose fractionated x-rays in 1930s-1950s and were followed-up for death from non-cancer causes during 1950–1987. In the current analysis, we scrutinized the assumption of linearity by analyzing a series of radio-biologically motivated nonlinear dose-response models to get a better understanding of the impact of radiation damage on IHD. The models were weighted according to their quality of fit and were then mathematically superposed applying the multi-model inference (MMI) technique. Our results indicated an essentially linear dose-response relationship for IHD mortality at low and medium doses and a supra-linear relationship at higher doses (>1.5 Gy). At 5 Gy, the estimated radiation risks were 5-fold higher compared to the linear-no-threshold (LNT) model. This is the largest study of patients exposed to fractionated low-to-moderate doses of radiation. Our analyses confirm previously reported significantly increased radiation risks of IHD from doses similar to those from diagnostic radiation procedures. International radiation protection organizations should evaluate potential underestimation of IHD risks at higher doses.

Ionizing radiation; ischemic heart diseases; LNT model; multi-model inference; nonlinear dose-responses

One of the most important questions in radiation research relates to the shape of the dose-response for different detrimental health outcomes at low exposures levels. Various international radiation protection organizations use the linear no-threshold (LNT) model to predict risks of cancer after ionizing radiation (IR) exposures (1-2). However, the most recent analysis of the Life Span Study (LSS) data suggests a significant quadratic upward curvature, especially for the incidence of all solid cancers in males (3). For cardiovascular diseases (CVDs), doses above 5 Gy IR have been shown to be associated with a significantly elevated risk (4). At doses between 0.5 and 5 Gy, there is clear evidence for an increased risk (4-8). Radiation risks at low (<0.1 Gy) and low-to-moderate (0.1-0.5 Gy) doses have been examined only in a few studies with considerable discrepancies in findings and require further research (9-19). In this context, the question whether even smallest doses of IR may increase the risk of CVDs or whether nonlinear dose-response curves may be better suited to describe the health risk is of special interest. There could also be a threshold for the dose below which radiation may have no effect, or lead to either a strongly elevated risk or a protective effect. Such questions are of great importance for radiation protection, especially against the rising worldwide use of IR in medical applications. They are also relevant for occupationally exposed groups of individuals. For CVDs, the question of the shape of the dose-response is as important as it is for cancer because even though radiation risk of CVDs are smaller than radiation risks of cancer (13), the overall burden of disease is much larger due to high background rates of CVDs in Western populations (20).

Recently significantly elevated risks of death from IHD in a cohort of tuberculosis patients from Canada exposed to low-to-moderate doses of highly-fractionated x-ray radiation from repeated chest fluoroscopies were reported (21). The reported dose-response was strictly linear, and researchers described a novel finding of a significant inverse dose-

fractionation association in IHD mortality (21). The aim of the present study is to investigate radiation-associated risk of IHD in the Canadian Fluoroscopy Cohort Study (CFCS) with a larger set of radio-biologically motivated dose-response models and to comprehensively characterize model uncertainties using multi-model inference (MMI, 22-24).

METHODS

Data Sources

The CFCS data have been described in detail elsewhere (21). The cohort includes 63,707 tuberculosis patients from Canada who were first treated for tuberculosis between 1930 and 1952 and could have received multiple fluoroscopic x-ray examinations to maintain pneumothorax, one of the preferred treatments in the pre-antibiotic era. Absorbed lung doses from fluoroscopy were estimated for each patient for each year since first admission for treatment of tuberculosis (25). The lung dose is the central dose measurement of interest as a reasonable surrogate for doses to the heart and associated major blood vessels. Thirty-nine percent of the cohort (24,932 patients) were exposed to at least one fluoroscopy while the remaining 38,775 are considered unexposed to radiation from fluoroscopy. On average, exposed patients were treated 64 times with a typical fluoroscopic examination delivering a mean lung dose of 0.0125 Gy at a dose-rate of approximately 0.6 mGy/second. The mean cumulative person-year-weighted lagged lung dose among exposed was 0.79 Gy (range, 0 - 11.6 Gy).

Study participants had to be alive at the start of follow-up in 1950 and were followed up for mortality until the end of 1987 with 1,902,251.68 person-years. During this time, 5,818

deaths from IHD (ICD-9 codes 410–414 und 429.2) were identified through a linkage with the Canadian Mortality Database. The cohort was evenly split between men and women. Patient age at first admission for tuberculosis treatment ranged from 1 to 81 years. Additional characteristics of the CFCS are provided in Web Table 1.

Statistical Methods

The present analysis applied the same dataset cross-classified by sex, Canadian province of most admissions, type of tuberculosis diagnosis, stage of tuberculosis, smoking status, age at first exposure, attained age, calendar year at risk, duration of fluoroscopy screenings, and 10-year cumulative lagged lung dose as (21). Poisson regression was based on time-dependent person-year–weighted mean cumulative dose in cross-classified cells, using excess relative risk (ERR) models in combination with a parametric baseline model. The general form of an ERR model is $h = h_0 \times (1+ERR(D, Z))$, where h is the total hazard function, h_0 is the parametric baseline model. $ERR(D, Z)$ describes the change of the hazard function with cumulative lagged lung dose D allowing for dose-effect modification by co-factor(s) Z, such as sex, age at first exposure or dose fractionation so that $ERR(D, Z) = err(D) \times \varepsilon(Z)$. Here, $err(D)$ represents the dose-response and $\varepsilon(Z)$ contains the dose-effect modifiers (DEMs). A parametric baseline model had been developed to analyze the risk for IHD in the Mayak Workers Cohort (17). It was taken as guidance for developing a parametric baseline model for the CFCS data. Both models for cohorts Mayak and CFCS are provided in Web Appendices 1 and 2. The baseline model in equation (A4) was combined with the LNT model and adjusted for dose-fractionation (21):

$$h = h_0\{1 + \beta_1 \times D \times \exp[\beta_2(drate - 0.2)]\} \quad (1)$$

Here, β_1 denotes the slope of the linear dose-response and β_2 is the parameter associated with the DEM *drate*-0.2. Parameter *drate* represents the dose fractionation, a surrogate for dose rate, defined as *drate*:= *D*/*time* where *time* is the overall duration of fluoroscopy treatments. The unit of *drate* is Gy/year. By centering *drate* parameter β_1 corresponds to the risk for a patient with radiation exposures at 0.2 Gy/yr, i.e. approximately 16 fluoroscopic procedures per year (21).

Subsequently, the dose-response model from equation (1) (i.e. $\beta_1 \times D$) was substituted by the models in Figure 1 (Q-model – Gompertz model). They were chosen with care to reflect as many biologically plausible shapes for dose-responses as possible, including supralinear and sublinear models. Mathematical details of all models in Figure 1 are provided in Web Appendix 3. The threshold-dose parameter (D_{th}) contained in some models (LTH, smooth step, sigmoid, hormesis, two-line spline) was optimized during the model fits. The smooth step model was implemented as a modified hyperbolic tangent function. With this function, a step is not imposed *a priori* but results from fitting that model to data.

Multi-model inference (MMI) method

The term MMI was coined to describe a frequentist approach to model averaging (22), and has been applied to model selection in radiobiology. In contrast to Bayesian model averaging (BMA) (26), which is based on the evaluation of model-specific marginal likelihood functions to determine a model average, MMI relies on AIC-based model weights for model building. BMA is computationally more demanding and only a few radiation epidemiological studies have used it to account for uncertainties in dose estimation (27-29). Both BMA and

MMI apply the concept of Occam's group (26, 30-32), where a group of models deemed adequate for averaging is selected from a larger group of candidate models (see Figure 1). The methods of picking models for Occam's group can vary. For example, Walsh and Kaiser (24) selected all published models, which have been applied to the same LSS dataset for the same endpoint, whereas Kaiser and Walsh (32) developed a rigorous selection process based on likelihood ratio tests (LRTs).

MMI provides both a more accurate determination of the dose-response and a more comprehensive characterization of model uncertainties by accounting for possible bias from model selection. It is a statistical method of superposing different models that all describe a certain data set about equally well (22, 23). In the present study the MMI approach aims to detect nonlinearities in the dose-response by combining biologically-plausible dose-responses based on goodness-of-fit.

Model selection

To assess the influence of model selection criteria on the risk estimates, we used two approaches. In the *sparse model approach,* candidate dose-response models from Figure 1 were compared using LRT at a 95% confidence level. With this method, a small set of final non-nested models with highly significant dose-responses was identified for Occam's group. Specifically, for each final non-nested model we calculated Akaike Information Criterion (AIC; 33, 34) using the formula:

$$AIC = dev + 2 \times N_{par},$$

where N_{par} is the number of model parameters. Models with smaller AIC are favored based on fit (via dev) and parameter parsimony (models with more parameters get punished by the

factor $2\times N_{par}$) (35). For a set of final non-nested models, AIC-weights are calculated; models with smaller AIC are assigned a larger weight (see Web Appendix 4). The resulting weights, multiplied by a factor of 10^4, gave a number of samples for risk estimates to be generated by uncertainty distribution simulations. We then combined model-specific probability density functions into one dataset. The resulting probability density distribution represents all uncertainties arising from the different models and their superposition. Central risk estimates from MMI were calculated from AIC-weighted maximum likelihood estimates (MLEs) for single risk models. 95% CI were derived from the final merged MMI probability density distributions.

In the second, *rich model approach*, an LRT-based reduction of dose-response parameters of the candidate models was not performed. The AIC was calculated for each different model fit together with the AIC-weights. Models with bilateral AIC-weights smaller than 5% did not survive the selection process; all others were included into the set of final non-nested models. This approach leads to a larger number of models deemed suitable for MMI. The calculation of AIC-weights for the two sets (or Occam's groups) of dose-response models based on both approaches ("sparse" versus "rich") is detailed in Web Appendix 4. The software used to perform the analysis is briefly introduced in Web Appendix 5.

RESULTS

Similarly to the previously published results (21), the slope parameter β_1 was not significant without adjustment for dose fractionation (β_1 = -0.046 Gy^{-1}, Table 1). Adjustment led to a significant *ERR* per dose = 0.182 Gy^{-1} with 95% CI: 0.049, 0.325 (Table 1) (*ERR* per dose =

0.176 Gy^{-1} in (21)). Subsequently, the LNT model from equation (1) was substituted by all other models from Figure 1, keeping the DEM *drate* - 0.2.

Table 2 summarizes the goodness-of-fit for 11 dose-response models. The Gompertz model had the best fit to the data (Table 2). Both Q and Gompertz models predicted no increase in risk below 0.05 Gy (Figure 4). While both models predicted a sublinear dose-response at low and medium doses up to ~1 Gy, the two-line spline model predicted a risk higher than all other models (Figures 2 and 3). The *ERR* predictions from MMI and LNT model at 0.1 Gy and 1 Gy are identical within their 95 % confidence intervals (Table 3). Consequently, up to 1 Gy both models (LNT and MMI) predict very similar excess cases (Table 4).

Considering the relations in Web Figure 1 and a *sparse model approach,* four final non-nested models survived the selection process and were included into Occam's group: LNT, Q, two-line spline and the Gompertz models. For these four models, the model parameters (baseline and radiation-associated), their MLEs and symmetric, Wald-type standard errors are provided in Web Table 2. Details related to model selection according to the *sparse* model approach are provided in Web Appendices 4 and 6 and Web Table 3.

According to the *rich model approach,* 10 models survived the selection process and contributed to MMI with normalized weights provided in Table 2. Figure 2 shows the *ERR* plotted against the cumulative lagged lung dose for the four final non-nested models and for the simulated dose-response curve from MMI, calculated with the *sparse* and the *rich* model approaches. Figures 3 and 4 show the best models and MMI for doses <2 and 0.1 Gy, respectively. Table 3 provides risk predictions based on MMI (*sparse*) and the LNT, Q, two-line spline and Gompertz models. The radiation-associated excess cases according to the four final non-nested models and MMI (*sparse*) are presented in Table 4.

The dose-response from MMI (*sparse*) is roughly linear at low doses (Figure 3). At low and medium doses up to ~1 Gy, MMI and the LNT model predict similar risk values (Figure 3 and Table 3). At doses >1.5 Gy, the dose-response from MMI predicted a considerably higher risk compared to the LNT model (Figures 2 and 3, Table 3). For the entire dose range, the dose-responses from the MMI calculated using both the *sparse* and the *rich* model approaches were similar to each other (Figures 2 to 4), e.g., at 1 Gy, MMI predicted an *ERR* of 0.216 with 95 % CI: 0.062, 0.48 and *ERR* = 0.218 with 95 % CI: 0.058, 0.473.

DISCUSSION

CFCS is the largest cohort of patients exposed to fractionated low-to-moderate doses of IR via fluoroscopic x-rays. About 15.5% of exposed CFCS patients were exposed to doses <0.1 Gy and thus provide direct evidence of possible risks from low-dose exposures such as CT scans (like fluoroscopic examinations, CT scans in their most commonly known form apply x-rays). We examined 10 biologically-plausible dose-response models together with a categorical model. At low and medium doses the MMI technique predicted an almost linear dose-response.

While the *sparse* model selection approach led to a set of four final non-nested models, the *rich* model approach yielded an Occam's group that contained ten out of the eleven dose-response models that were fitted to the data. Both sets of dose-response models describe the data approximately equally well (see values of ΔAIC in Table 2).

The reason for MMI-predicted risks being significantly higher compared to the LNT model at doses >1.5 Gy is the relatively strong contributions of the Q, two-line spline and

Gompertz models to the MMI (88 % of the total, Table 2). At 5 Gy, MMI predicted an approximately 5-fold risk compared to the LNT model, at 10 Gy a 6-fold risk.

To better understand predicted radiation risks at higher doses, we used a restriction analysis and observed that the second slope of the two-line spline model (β_2) was driven by high doses (>2 Gy). When restricting the data to doses smaller than 2 Gy, the first slope (β_1) of this model became very similar to the slope of the LNT model (results not shown). The LNT model was influenced mostly by doses <2 Gy. The higher doses hardly influence the slope of the LNT model due to the lower number of cases in this dose range (212 cases out of 5,818). Thus, the fit of the two-line spline model, which predicts an almost twice as higher number of excess cases than the LNT model (Table 4), is consistent with the fit of the latter model.

The present study applied a larger range of biologically-realistic smooth dose-response models, including a hormesis model (Figure 1) (36). Exploring a larger range of different dose-response models is motivated by the following biological findings. Dose-responses which allow for protective effects at low doses, such as LQ, hormesis and two-line spline models, can be justified from mouse studies (10, 11). They found U-shaped and J-shaped dose-responses in ApoE-/- mice for biological endpoints associated with atherosclerosis. Low-dose induced anti-inflammatory effects which play an important role in that context are currently intensely studied (see e.g. the reviews 37-39) and have also been reported in (40, 41). Earlier, low doses of γ-radiation delivered at low dose-rates exhibited a protective effect related to chronic ulcerative dermatitis, an inflammatory skin reaction, in C57BL/6 mice, decreasing both disease frequency and severity and extending the lifespan of older animals (42). LTH models are another realistic possibility for dose-responses related to radio-epidemiological cohorts given the findings from animal studies on protective anti-

inflammatory effects induced by low doses of radiation (10, 11, 40, 41). Mathias et al. (41) provided evidence for anti-inflammatory effects after low-dose exposure but also found some pro-inflammatory responses. In such a situation, a LTH model may describe the data better than the LNT model. Interestingly, Mitchel et al. (42) reported that their dermatitis data indicate that low doses may generally produce either no effect or protective effects with respect to this autoimmune- and age-related non-cancer disease in mice. The finding of anti-inflammatory protective effects at low doses and detrimental effects at moderate (0.3 Gy) and higher doses (6 Gy) (43) provides a biological context for applying the smooth step model (Figure 1). A step-type response (with a steep slope) may reflect the distinct dose at which protective mechanisms are lost. Different tissues and different individuals can be expected to have different threshold-doses, leading to an overall smooth transition. While at low doses it is feasible that risk increase may be balanced by a protective decrease as in the LTH model, a smooth transition zone may exist where risk increases steadily, followed by a plateau.

At low and medium doses our results are in agreement with the earlier findings (21) and based on a more comprehensive analysis with a larger series of biologically-plausible dose-responses. An essential difference with the primary analysis (21) is the use of a different baseline model. The present study applied the parametric baseline model given in equation (A4) of Web Appendix 2 with 21 baseline parameters while in (21) a stratified baseline model with one free parameter for each possible combination of available categories in the data was used. Their baseline model contained several thousand free parameters and was not suitable for AIC-based MMI analysis for which parsimony in parameters is essential (24).

In a recent MMI-based analysis of the LSS mortality data for heart diseases observed during 1950-2003 an *ERR* of 0.08 at 1 Gy with 95 % CI: (0, 0.20) was reported (16). Shimizu et al. (2010) reported an *ERR* per dose of 0.14 with 95% CI: (0.06, 0.23). Within the error

bars these values are roughly consistent with our estimate of 0.216 at 1 Gy with 95% CI: 0.062, 0.48. The latest analysis of the LSS mortality data with extended follow-up from 1950-2008 found no significant association between radiation exposure and IHD (18). For IHD mortality in male Mayak workers, an *ERR* per dose of 0.09 Gy^{-1} with 95% CI: 0.02, 0.16 was reported (17). This value is consistent with the risk prediction from the present study. For females, no significant elevation in risk was found (17). Azizova et al. (6) did not find a significant association of total dose from external γ-rays with IHD mortality in Mayak workers. For a mean heart dose of 5 Gy after radiotherapy for breast cancer an *ERR* of 0.37 with 95 % CI: (0.15, 0.73) was reported (44). That is considerably lower than our MMI estimate for 5 Gy (*ERR* = 4.70 at 5 Gy with 95 % CI: 0.60, 10).

There remains considerable controversy over the effects of dose protraction on long-term health outcomes. Survivors of atomic bombings in Hiroshima and Nagasaki were exposed to acute exposure and could not provide useful information on the effects of dose-fractionation. Limited data exist on the dose-rate effects in Mayak workers, primarily in the form of annual absorbed doses. In contrast, the CFCS has detailed exposure information on the dose and dose-rate of a typical fluoroscopic examination and number of fluoroscopic procedures for each patient per year. Altogether, the CFCS is the largest study of patients exposed to moderately fractionated low-to-moderate doses of IR and presents one of the most valuable cohorts worldwide to derive information related to radiation effects at low, moderate and high doses of IR.

For IHD mortality among nuclear workers an *ERR* per dose of 0.18 Sv^{-1} with 90 % CI: (0.004, 0.36) was reported (19). Recently, the CFCS data for IHD (21) were combined with a cohort of tuberculosis fluoroscopy patients from Massachusetts and analyzed with a linear dose-response model applying two different dose regimes with a cut-point at 0.5 Gy

(45). The authors reported increasing trends for doses <0.5Gy, over the entire dose range a negative dose trend was observed (45). This is probably due to the inability to adjust for dose-fractionation effects in the Massachusetts data where only cumulative doses to the lung have been estimated. The present study used a more comprehensive and flexible approach by analyzing the data with a variety of different linear and non-linear models including those that exhibit flexible threshold-doses without applying artificial cut-points at certain doses and without relying on LNT as a foregone conclusion (12, 46).

In summary, the present study confirms previous findings in a number of studies of essentially linear dose-response for death from IHD at low and moderate doses (0 – 1 Gy). Our analyses suggest that different biological mechanisms may operate at low and medium doses compared to high doses and that at higher doses, the LNT model underestimates the risk compared to the dose-response from MMI by a factor of 5. Our results should be of particular interest to international radiation protection organizations, which largely rely on analyses of radio-epidemiological cohorts using the LNT model. We conclude that our findings have important implications for risk assessment of IR in the context of medical applications (such as CT scans, radiotherapy and low dose anti-inflammatory radiotherapy), nuclear energy production and accident related long term risks.

REFERENCES

1. International Commission on Radiological Protection. *Low-dose Extrapolation of Radiation-related Cancer Risk. ICRP Publication 99*. Ann. ICRP. 2005;35(4).

2. UNSCEAR 2000 Report Vol. II. *Sources and Effects of Ionizing Radiation*. United Nations Scientific Committee on the Effects of Atomic Radiation. UNSCEAR 2000 Report to the General Assembly, with scientific annexes

3. Grant EJ, Brenner A, Sugiyama H, et al. Solid Cancer Incidence among the Life Span Study of Atomic Bomb Survivors: 1958-2009. *Radiat Res*. 2017;187(5):513-537.

4. Health Protection Agency. *Circulatory disease risk. Report of the Independent Advisory Group on Ionising Radiation*. London: Health Protection Agency; 2010 (ISBN 978-0-85951-676-1).

5. Kreuzer M, Auvinen A, Cardis E, et al. Low-dose ionising radiation and cardiovascular diseases--Strategies for molecular epidemiological studies in Europe. *Mutat Res Rev Mutat Res*. 2015;764:90-100.

6. Azizova TV, Grigoryeva ES, Haylock RG, et al. Ischaemic heart disease incidence and mortality in an extended cohort of Mayak workers first employed in 1948-1982. *Br J Radiol*. 2015;88(1054):20150169.

7. Azizova TV, Grigorieva ES, Hunter N, et al. Risk of mortality from circulatory diseases in Mayak workers cohort following occupational radiation exposure. *J Radiol Prot*. 2015;35(3):517-538.

8. Moseeva MB, Azizova TV, Grigoryeva ES, et al. Risks of circulatory diseases among Mayak PA workers with radiation doses estimated using the improved Mayak Worker Dosimetry System 2008. *Radiat Environ Biophys*. 2014;53(2):469-477

9. Shimizu Y, Kodama K, Nishi N, et al. Radiation exposure and circulatory disease risk: Hiroshima and Nagasaki atomic bomb survivor data, 1950–2003. *Brit Med J*. 2010;340:b5349.

10. Mitchel RE, Hasu M, Bugden M, et al. Low-dose radiation exposure and atherosclerosis in ApoE–/– mice. *Radiat Res*. 2011;175:665–676.

11. Mitchel RE, Hasu M, Bugden M, et al. Low-dose radiation exposure and protection against atherosclerosis in ApoE(-/-) mice: the influence of P53 heterozygosity. *Radiat Res*. 2013;179(2):190-199.

12. Little MP, Azizova TV, Bazyka D, et al. Systematic review and meta-analysis of circulatory disease from exposure to low-level ionizing radiation and estimates of potential population mortality risks. *Environ Health Perspect*. 2012;120(11):1503–1511.

13. Ozasa K, Shimizu Y, Suyama A, et al. Studies of the mortality of atomic bomb survivors, Report 14, 1950-2003: an overview of cancer and noncancer diseases. *Radiat Res*. 2012; 177(3):229-243.

14. Ozasa K, Takahashi I, Grant EJ, et al. Cardiovascular disease among atomic bomb survivors. *Int J Radiat Biol*. 2017;93(10):1145-1150.

15. Schöllnberger H, Kaiser JC, Jacob P, et al. Dose-responses from multi-model inference for the non-cancer disease mortality of atomic bomb survivors. *Radiat Environ Biophys*. 2012; 51(2):165-178.

16. Schöllnberger H, Eidemüller M, Cullings HM, et al. Dose-responses for mortality from cerebrovascular and heart diseases in atomic bomb survivors: 1950-2003. *Radiat Environ Biophys*. 2018;57(1):17-29.

17. Simonetto C, Azizova TV, Grigoryeva ES, et al. Ischemic heart disease in workers at Mayak PA: Latency of incidence risk after radiation exposure. *PLoS One*. 2014;9(5):e96309.

18. Takahashi I, Shimizu Y, Grant EJ, et al. Heart Disease Mortality in the Life Span Study, 1950-2008. *Radiat Res*. 2017;187(3):319-332.

19. Gillies M, Richardson DB, Cardis E, et al. Mortality from Circulatory Diseases and other Non-Cancer Outcomes among Nuclear Workers in France, the United Kingdom and the United States (INWORKS). *Radiat Res*. 2017;188(3):276-290.

20. World Health Organization. *Fact sheet no. 310. The top 10 causes of death*. Geneva, Switzerland: World Health Organization; 2013. Available at http://who.int/mediacentre/factsheets/fs310/en/index.html

21. Zablotska LB, Little MP, Cornett RJ. Potential increased risk of ischemic heart disease mortality with significant dose fractionation in the Canadian Fluoroscopy Cohort Study. *Am J Epidemiol*. 2014;179(1):120-131.

22. Burnham KP, Anderson DR. *Model selection and multimodel inference*. 2nd ed. New York: Springer; 2002.

23. Claeskens G, Hjort NL. Model selection and model averaging. Cambridge: Cambridge University Press; 2008.

24. Walsh L, Kaiser JC. Multi-model inference of adult and childhood leukaemia excess relative risks based on the Japanese A-bomb survivors mortality data (1950–2000). *Radiat Environ Biophys*. 2011;50(1):21–35.

25. Miller AB, Howe GR, Sherman GJ, et al. Mortality from breast cancer after irradiation during fluoroscopic examinations in patients being treated for tuberculosis. *N Engl J Med*. 1989;321(19):1285–1289.

26. Hoeting JA, Madigan D, Raftery AE, et al. Bayesian model averaging: a tutorial. *Statist Sci*. 1999;14(4):382–417.

27. Land CE, Kwon D, Hoffman FO, et al. Accounting for shared and unshared dosimetric uncertainties in the dose response for ultrasound-detected thyroid nodules after exposure to radioactive fallout. *Radiat Res*. 2015;183(2):159-173.

28. Little MP, Kukush AG, Masiuk SV, et al. Impact of uncertainties in exposure assessment on estimates of thyroid cancer risk among Ukrainian children and adolescents exposed from the Chernobyl accident. *PLoS One*. 2014;9(1):e85723.

29. Little MP, Kwon D, Zablotska LB, et al. Impact of Uncertainties in Exposure Assessment on Thyroid Cancer Risk among Persons in Belarus Exposed as Children or Adolescents Due to the Chernobyl Accident. *PLoS One*. 2015;10(10):e0139826.

30. Madigan D, Raftery AE. Model selection and accounting for model uncertainty in graphical models using Occam's window. *J Amer Statist Assoc*. 1994; 89(428):1535–1546.

31. Noble RB, Bailer AJ, Park R. Model-Averaged Benchmark Concentration Estimates for Continuous Response Data Arising from Epidemiological Studies. *Risk Anal*. 2009;29(4):558-564.

32. Kaiser JC, Walsh L. Independent analysis of the radiation risk for leukaemia in children and adults with mortality data (1950-2003) of Japanese A-bomb survivors. *Radiat Environ Biophys*. 2013;52(1):17-27.

33. Akaike H. In: Petrov BN, Caski F, eds. Information theory and an extension of the maximum likelihood principle. Proceedings of the second international symposium on information theory. Akademiai Kiado, Budapest; 1973: 267–281.

34. Akaike H. A new look at the statistical model identification. *IEEE Trans Autom Control*. 1974;19(6):716–723.

35. Walsh L. A short review of model selection techniques for radiation epidemiology. *Radiat Environ Biophys*. 2007;46(3):205-213.

36. Brain P, Cousens R. An equation to describe dose responses where there is stimulation of growth at low doses. *Weed Res.* 1989;29:93–96.

37. Rödel F, Frey B, Gaipl U, et al. Modulation of inflammatory immune reactions by low-dose ionizing radiation: molecular mechanisms and clinical application. *Current Medicinal Chemistry* 2012a;19(12):1741-1750.

38. Rödel F, Frey B, Manda K, et al. Immunomodulatory properties and molecular effects in inflammatory diseases of low-dose x-irradiation. *Front Oncol*. 2012b; 2:1-9.

39. Frey B, Hehlgans S, Rödel F, et al. Modulation of inflammation by low and high doses of ionizing radiation: Implications for benign and malign diseases. *Cancer Lett*. 2015; 368(2):230-237.

40. Le Gallic C, Phalente Y, Manens L, et al. Chronic internal exposure to low dose 137Cs induces positive impact on the stability of atherosclerotic plaques by reducing inflammation in ApoE-/- Mice. *PLoS One*. 2015;10(6):e0128539.

41. Mathias D, Mitchel RE, Barclay M, et al. Low-dose irradiation affects expression of inflammatory markers in the heart of ApoE -/- mice. *PLoS One*. 2015;10(3):e0119661.

42. Mitchel RE, Burchart P, Wyatt H. Fractionated, low-dose-rate ionizing radiation exposure and chronic ulcerative dermatitis in normal and Trp53 heterozygous C57BL/6 mice. *Radiat Res*. 2007;168(6):716-724.

43. Mancuso M, Pasquali E, Braga-Tanaka I 3rd, et al. Acceleration of atherogenesis in ApoE-/- mice exposed to acute or low-dose-rate ionizing radiation. *Oncotarget*. 2015;6(31):31263-31271.

44. Darby SC, Ewertz M, McGale P et al. Risk of ischemic heart disease in women after radiotherapy for breast cancer. *N Engl J Med*. 2013;368(11):987-998.

45. Tran V, Zablotska LB, Brenner AV, et al. Radiation-associated circulatory disease mortality in a pooled analysis of 77,275 patients from the Massachusetts and Canadian tuberculosis fluoroscopy cohorts. *Sci Rep*. 2017;7:44147.

46. Little MP. Radiation and circulatory disease. *Mutat Res*. 2016;770(Pt B):299-318.

FIGURE LEGENDS

Figure 1: Typical shapes of the functions that were used to analyze the dose-response for IHD mortality in the Canadian Fluoroscopy Cohort Study (follow-up 1950–1987). 1st row: linear no-threshold (LNT) model, quadratic (Q), linear-quadratic (LQ); 2nd row: linear-exponential (LE) model, linear threshold (LTH), smooth step model; 3rd row: sigmoid model, hormesis model, two-line spline model; 4th row: Gompertz model, categorical model. Additional dashed lines show the flexibility of some of the models.

Figure 2: *ERR* for IHD mortality in the Canadian Fluoroscopy Cohort Study (follow-up 1950–1987) versus cumulative lagged lung dose for the four final non-nested ERR models (Table 2) and the simulated dose-response curves from MMI, calculated with the *sparse* model approach and the *rich* model approach. The shaded area represents the 95% CI region for the MMI (*sparse* model approach). For AIC-weights see the insert. The dotted straight line shows the risk prediction from (21). The figure is valid for males and females. A dose-fractionation of 0.2 Gy/year was assumed. Online version contains color.

Figure 3: *ERR* for IHD mortality in the Canadian Fluoroscopy Cohort Study (follow-up 1950–1987) versus cumulative lagged lung dose up to 2 Gy for the four final non-nested ERR models (Table 2) and the simulated dose-response curves from MMI, calculated with the *sparse* model approach and the *rich* model approach. Vertical dotted lines represent the 95% CI region for the MMI (*sparse* model approach). For AIC-weights see the insert. The dotted straight line shows the risk prediction from (21). The figure is valid for males and females. A dose-fractionation of 0.2 Gy/year was assumed. Online version contains color.

Figure 4: *ERR* for IHD mortality in the Canadian Fluoroscopy Cohort Study (follow-up 1950–1987) versus cumulative lagged lung dose up to 0.1 Gy for the four final non-nested ERR models (Table 2) and the simulated dose-response curves from MMI, calculated with the *sparse* model approach and the *rich* model approach. Vertical dotted lines represent the 95% CI region for the MMI (*sparse* model approach). For AIC-weights see the insert. The dotted straight line shows the risk prediction from (21). The figure is valid for males and females. A dose-fractionation of 0.2 Gy/year was assumed. Online version contains color.

Figure 1

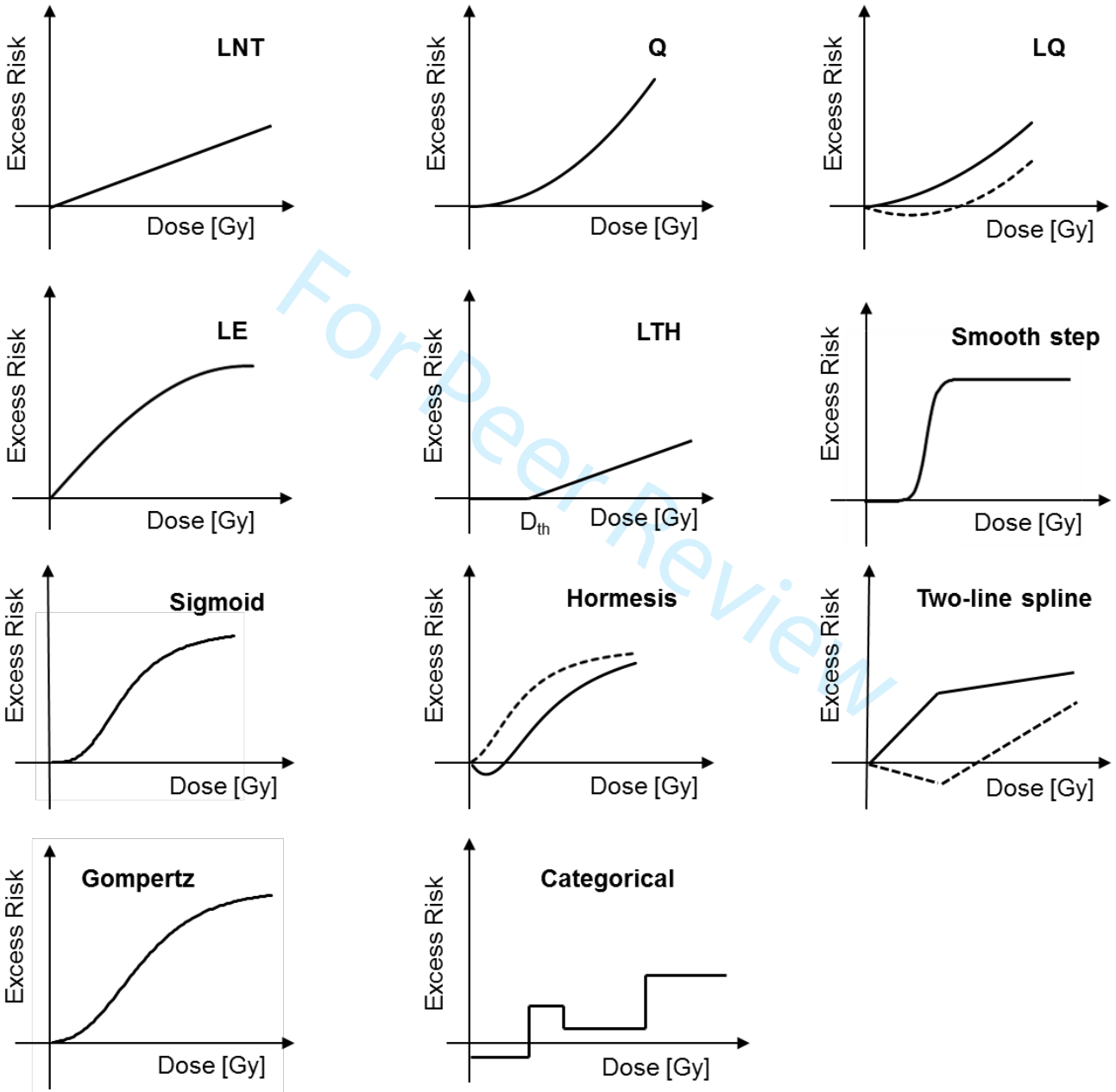

Figure 2

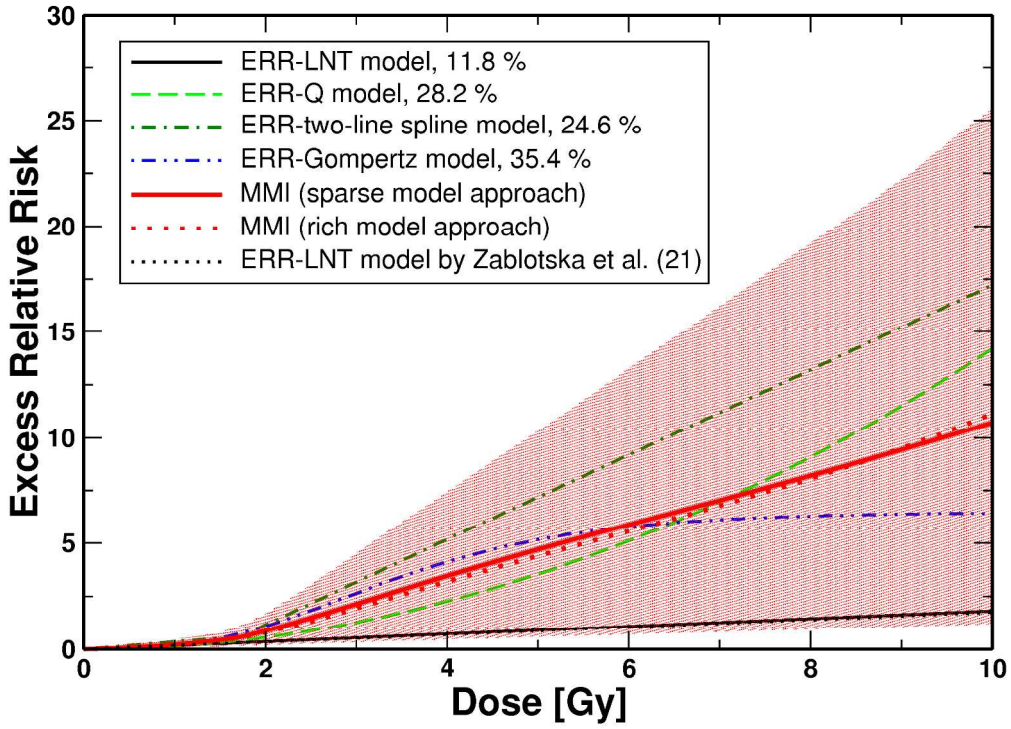

Figure 3

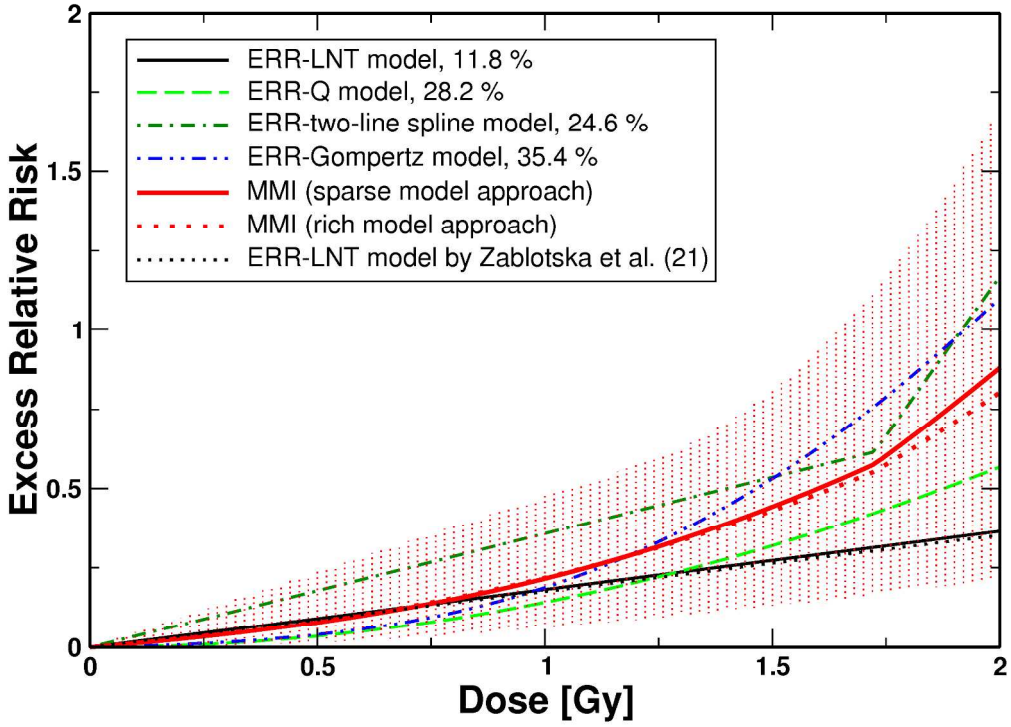

Figure 4

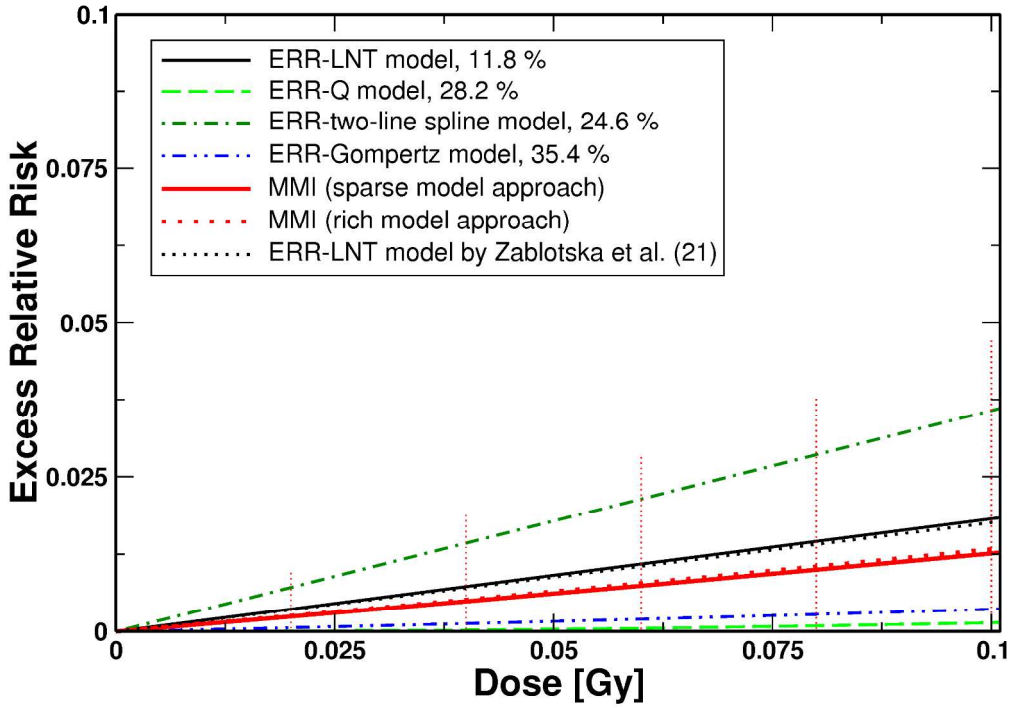

Table 1. MLEs of Model Parameters, Related 95% CIs and Final Deviances of Fitting ERR-LNT Models to the Mortality Data for IHD (Zablotska et al. (21)), Canadian Fluoroscopy Cohort Study, 1950-1987

Parameter	Zablotska et al. (21), LNT model without dose-fractionation adjustment[a]	Zablotska et al. (21), LNT model with dose-fractionation adjustment[a]	Present study, LNT model without dose-fractionation adjustment[a,b]	Present study, LNT model with dose-fractionation adjustment[a,c,d]
β_1	0.007 Gy^{-1} (-0.044, 0.072)	0.176 Gy^{-1} (0.011, 0.39)	-0.046 Gy^{-1} (-0.075, -0.013)	0.182 Gy^{-1} (0.049, 0.33)
β_2		-10.2 years Gy^{-1} (-25, -2.1)		-12.0 years Gy^{-1} (-21, -5.1)
dev	9884.50	9879.76	13250.95	13247.75

Abbreviations: CI, confidence interval; dev, final deviance; ERR-LNT, linear no-threshold model implemented as excess relative risk model; IHD, ischemic heart diseases; MLE, maximum likelihood estimate.

[a] The difference between the model applied by Zablotska et al. (21) and the one from the present study is the baseline model (stratified in the first case, parametric in the present study; see Web Appendix 5).

[b] Fit was performed with model given in equation (1) with $\beta_2 = 0$.

[c] Fit was performed with model given in equation (1).

[d] As a comparison, the fit of the parametric baseline model alone with its 21 parameters led to dev = 13252.68.

Table 2. Results of Fitting the Dose-Response Models From Figure 1 as ERR Models to the Mortality Data for IHD (Zablotska et al. (21)), Canadian Fluoroscopy Cohort Study, 1950-1987

	dev[a]	Δdev[b]	N_{par}	AIC[c]	ΔAIC[d]	Normalized Akaike weights, sparse model approach[e]	Normalized Akaike weights, rich model approach[f]
ERR-LNT	13247.75	6.19	23	13293.75	2.19	0.1183	0.0776
ERR-Q	13246.01	4.46	23	13292.01	0.46	0.2815	0.1847
ERR-LQ	13245.38	3.83	24	13293.38	1.83		0.0930
ERR-LE	13245.68	4.13	24	13293.68	2.13		0.0802
ERR-LTH, D_{th} = 0.58 Gy	13246.81	5.26	24	13294.81	3.26		0.0455
ERR-smooth step, D_{th} = 4,47 Gy	13244.45	2.90	25	13294.45	2.90		0.0546
ERR-sigmoid, D_{th} = 41,53 Gy	13245.94	4.39	25	13295.94	4.39		0.0259
ERR-hormesis, D_{th} = 3,28 Gy	13242.84	1.29	26	13294.84	3.29		0.0449
ERR-two-line spline, D_{th} = 1.72 Gy	13242.28	0.73	25	13292.28	0.73	0.2461	0.1615
ERR-Gompertz, D_{th} = 0	13241.55	0	25	13291.55	0	0.3541	0.2323
ERR-categorical	13242.19	0.63	29	13300.19	8.63		

Abbreviations: AIC, Akaike Information Criterion; dev, final deviance; ERR-LNT, linear no-threshold model implemented as excess relative risk model; ERR-Q, quadratic model implemented as excess relative risk model; ERR-LQ, linear-quadratic model implemented as excess relative risk model; ERR-LE, linear-exponential model implemented as excess relative risk model; ERR-LTH, linear-threshold model implemented as excess relative risk model.

[a] As a comparison, the fit of the baseline model alone with its 21 parameters led to dev = 13252.68.

[b] The difference in final deviance is denoted by Δdev with respect to the model with the smallest final deviance.

[c] AIC = dev + 2 × N_{par}, where N_{par} is the number of model parameters.

[d] The difference in AIC-values with respect to the model with the smallest AIC-values is denoted by ΔAIC.

[e] According to the sparse model approach four models survive the selection process and are used for MMI. The normalized Akaike weights provided here were calculated with equation (A5) from Web Appendix 4.

[f] According to the rich model approach all models except the categorical model survive the selection process because when compared to the model with ΔAIC = 0 they have an Akaike weight > 0.05. The normalized Akaike weights provided here were calculated with equation (A5) from Web Appendix 4.

Table 3. Values for *ERR* for Mortality from IHD (Zablotska et al. (21)) at Various Cumulative Lung Doses Calculated With MMI (Sparse Model Approach) and the Three Final Non-Nested Models, Canadian Fluoroscopy Cohort Study, 1950-1987

Lung dose (Gy)	MMI[a,b]	ERR-LNT model[b,c]	ERR-Q model[b]	ERR-two-line spline[b]	ERR-Gompertz[b]
0.1	0.01263 (0.00075; 0.048)	0.0182 (0.0045; 0.032)	0.0014 (0.00049; 0.0024)	0.036 (0.017; 0.054)	0.0036 (0.0013; 0.0060)
0.2	0.0266 (0.0028; 0.095)	0.0364 (0.0089; 0.064)	0.0057 (0.0020; 0.0094)	0.071 (0.035; 0.11)	0.0089 (0.0033; 0.015)
0.5	0.079 (0.016; 0.24)	0.091 (0.022; 0.16)	0.036 (0.012; 0.059)	0.179 (0.087; 0.27)	0.040 (0.015; 0.066)
1	0.216 (0.062; 0.48)	0.182 (0.045; 0.32)	0.142 (0.049; 0.24)	0.36 (0.17; 0.54)	0.188 (0.070; 0.31)
2	0.88 (0.21; 1.7)	0.364 (0.089; 0.64)	0.57 (0.20; 0.94)	1.17 (0.64; 1.7)	1.1 (0.41; 1.8)
5	4.70 (0.60; 10)	0.91 (0.22; 1.6)	3.6 (1.2; 5.9)	7.2 (2.3; 12)	5.2 (1.9; 8.5)
10	11 (1.2; 26)	1.82 (0.45; 3.2)	14.2 (4.9; 24)	17.2 (4.8; 30)	6.4 (2.4; 11)

Abbreviations: ERR-LNT, linear no-threshold model implemented as excess relative risk model; ERR-Q, quadratic model implemented as excess relative risk model; IHD, ischemic heart diseases; MMI, multi-model inference.

[a] Calculated with the sparse model approach.

[b] 95% confidence intervals are provided in parenthesis.

[c] As a comparison, the *ERR* per dose from Zablotska et al. (21) is 0.175 Gy^{-1} with 95% CI: 0.011, 0.393.

Table 4. Radiation-Associated Excess Cases for the Mortality Data for IHD (Zablotska et al. (21)) According to the Three Final Non-Nested Models and MMI (Sparse Model Approach), Canadian Fluoroscopy Cohort Study, 1950-1987

Dose-bin	MMI[a]	ERR-LNT	ERR-Q	ERR-two-line spline	ERR-Gompertz
0 - 0.05 Gy	2.8	5.7	0.2	7.4	0.6
0.05 - 0.1 Gy	1.1	2	0.2	2.7	0.3
0.1 - 0.2 Gy	1.3	2.2	0.3	3.3	0.3
0.2 - 0.3 Gy	2.8	4	0.8	7.5	0.7
0.3 - 0.4 Gy	2.6	3.8	1.1	6.4	0.7
0.4 – 0.5 Gy	3.6	4.8	1.8	8.4	1.4
0.5 – 0.75 Gy	8.9	10	4.6	20.2	4
0.75 - 1 Gy	11.5	11.7	7.2	23.1	6.9
1 - 1.5 Gy	19.7	15.6	12.3	33.9	17
1.5 – 2 Gy	14	8.9	9.4	19.9	15.2
2 - 3 Gy	18	6.2	8.2	32.6	19.7
3 - 4 Gy	7.8	2	3.8	13.3	9.1
4 - 5 Gy	3.3	0.7	1.7	5.4	3.9
5 Gy -	4.7	1.1	3.6	7.3	5
sum:	102.1	78.7	55.2	191.4	84.8

Abbreviations: ERR-LNT, linear no-threshold model implemented as excess relative risk model; ERR-Q, quadratic model implemented as excess relative risk model; IHD, ischemic heart diseases; MMI, multi-model inference.

[a] Calculated with the sparse model approach.

WEB MATERIAL

Radio-biologically Motivated Modeling of Radiation Risks of Mortality From Ischemic Heart Diseases in the Canadian Fluoroscopy Cohort Study

WEB APPENDIX 1: BASELINE MODEL OF SIMONETTO ET AL. (1) DEVELOPED FOR THE MAYAK WORKERS COHORT

$$h_0 = 10^{-5} \times e^{\psi_{cat} + \psi_{time} + \psi_{emigration}}$$

$$\psi_{cat} = \psi_{smoking} + \psi_{drinking} + \psi_{bmi} + \psi_{blood\ pressure} + \psi_{plant}$$

$$\psi_{time} = \psi_{age} + \psi_{birth} + \psi_{calendar} + \psi_{employment}$$

$$\psi_{emigration} = \varepsilon \times \Theta(b + a - m)$$

$$\psi_{age} = \psi_0 + \psi_1 \ln(\frac{a}{60}) + \psi_2 \ln^2(\frac{a}{60}) + \sum_i \alpha_i \ln^2(\frac{a}{\vartheta_{\alpha,i}})\Theta(a - \vartheta_{\alpha,i})$$

$$\psi_{birth} = \beta_1 \frac{b - 1900}{10} + \beta_2 \frac{(b - 1900)^2}{100}$$

$$\psi_{calendar} = \sum_i \gamma_i \frac{\mathrm{LT}(b + a - \vartheta_{\gamma,i})}{10} \qquad \text{(A1)}$$

$$\psi_{employment} = \delta_1 \frac{f - 1950}{10} + \delta_2 \frac{(f - 1950)^2}{100}$$

Here, h_0 is the baseline hazard, referred to in the main text as parametric baseline model. Summands in ψ_{cat} evaluate to zero for non-smoker, non-drinker, for persons with normal body mass index, normal blood pressure and for reactor workers. Otherwise they evaluate to some value determined by the fit. The lower case Greek symbols are free parameters. The quantities a, b, f and m denote attained age, birth date, date of first employment at Mayak Production Association (PA) and date of emigration from Ozyorsk, the closed city in which the Mayak workers have lived throughout the operation of the Mayak PA. The quantities $\vartheta_{\alpha,i}$ and $\vartheta_{\gamma,i}$ denote so called age knots. Furthermore, the Heaviside step function Θ was applied together with a function $\mathrm{LT}(t)$:

$$\Theta(t) = \begin{cases} 0 & \text{for } t < 0 \\ 1 & \text{for } t \geq 0 \end{cases} \qquad \mathrm{LT}(t) = \begin{cases} 0 & \text{for } t < 0 \\ t & \text{for } t \geq 0 \end{cases} \qquad \text{(A2)}$$

For some further explanations the reader is referred to the Appendix in Simonetto et al. (1).

WEB APPENDIX 2: BASELINE MODEL APPLIED IN THE PRESENT STUDY

The parametric baseline model that was applied in the present study is as follows.

$$h_0 = 10^{-4} \times e^{\psi_{cat} + \psi_{time}}$$

$$\psi_{cat} = \psi_{gender} + \psi_{province} + \psi_{duration} + \psi_{diagnosis} + \psi_{stage}$$

$$\psi_{time} = \psi_{age} + \psi_{birth} \qquad \text{(A3)}$$

$$\psi_{age} = \psi_1 \ln(\frac{a}{50}) + \sum_i \alpha_i \ln^2(\frac{a}{\vartheta_{\alpha,i}})\Theta(a - \vartheta_{\alpha,i})$$

$$\psi_{birth} = \beta_1 \frac{b-1900}{10} + \beta_2 \frac{(b-1900)^2}{100}$$

For all parameters a distinction according to sex was allowed for. The actual baseline model that was fitted to the CFCS data in the present study is as follows:

$$\begin{aligned} h_0 = 10^{-4} \times \exp\{ & c\_m + c\_f + prov\_m + prov\_f + cdur\_m + cdur\_f + \\ & diag\_m + diag\_f + nostg\_m + nostg\_f + \\ & stg1\_m + stg1\_f + stg2\_m + stg2\_f + stg3\_m + stg3\_f + \\ & ba\_m \times \ln(a/50) + ba\_f \times \ln(a/50) + \\ & basq\_m \times \ln^2(a/50) \times \Theta(a\text{-}50) + basq\_f \times \ln^2(a/50) \times \Theta(a\text{-}50) + \\ & bb\_m \times ((b\text{-}1900)/10) + bb\_f \times ((b\text{-}1900)/10) + \\ & bbsq\_m \times ((b\text{-}1900)^2/100) + bbsq\_f \times ((b\text{-}1900)^2/100)\} \end{aligned} \qquad \text{(A4)}$$

Model parameters in equation (A4) are italicised. The free parameters *c_m* and *c_f* relate to males and females, respectively. The free parameters *prov_m* and *prov_f* relate to males and females admitted to hospitals outside the Canadian province of Nova Scotia, respectively. The parameters *cdur_m* and *cdur_f* are associated with duration of fluoroscopy screenings in male and female patients, respectively. The parameters *diag_m* and *diag_f* relate to males and females with diagnosis pulmonary tuberculosis, respectively. Furthermore, *nostg_m* relates to male patients who – related to the stage of tuberculosis - contain the status not assigned (i.e. not specified). The parameter *stg3_f* is associated with females with advanced stage of tuberculosis. The free parameter *ba_m* describes the dependence of males on attained age *a*. In addition, *basq_m* relates to the quadratic age-dependence in males, associated with the term $\ln^2(a/50)\times\Theta(a\text{-}50)$. According to equation (A2) this expression is equal to $\ln^2(a/50)$ for attained ages larger or equal 50 years, otherwise it is zero. The remaining parameters are related to the linear and quadratic dependence from birth date *b*: *bb_m* and *bb_f*, for example, are the free parameters related to the linear dependence of male and female patients from birth year, respectively.

Because a limited amount of smoking information is available for only approximately 20% of the cohort, smoking was not included in the baseline model, in accordance with

Zablotska et al. (2). The baseline model in equation (A4) contains the same explanatory variables as the stratified baseline model applied by Zablotska et al. (2).

WEB APPENDIX 3: MATHEMATICAL FUNCTIONS USED FOR THE 11 PARAMETRIC DOSE-RESPONSE MODELS FROM FIGURE 1

The general form of an ERR model is $h = h_0 \times (1 + ERR(D, Z))$, where h is the total hazard function, h_0 is the baseline model and $ERR(D, Z)$ describes the change of the hazard function with dose D allowing for dose-modification by association-modifying factor(s) Z. It is $ERR(D, Z) = err(D) \times \varepsilon(Z)$. Here, $err(D)$ describes the shape of the dose-response function, $\varepsilon(Z)$ contains the DEMs. For h_0 the model in equation (A4) was applied.

For $err(D)$ the following dose-response models were used.

$err(D) = \beta_1 \times D$ LNT model

$err(D) = \beta_1 \times D^2$ Quadratic model

$err(D) = \beta_1 \times D + \beta_2 \times D^2$ Linear-quadratic model

$err(D) = \beta_1 \times D \times \exp(\beta_2 D)$ Linear-exponential model

$$err(D) = \begin{cases} 0 & \text{for } D < D_{th} \\ \beta_1 \times (D - D_{th}) & \text{for } D \geq D_{th} \end{cases}$$ Linear threshold model

$err(D) = 0.5 \times scale \times [\tanh(s\,(D - D_{th})) - \tanh(-s\,D_{th})]$ Smooth step model

$$err(D) = \lambda_0 \left(1 - \frac{1}{1 + \left(\frac{D}{D_{th}} \right)^{\lambda_1}} \right)$$ Sigmoid model

$$err(D) = \lambda_0 - \frac{\lambda_0 + \lambda_2 D}{1 + \left(\frac{D}{D_{th}} \right)^{\lambda_1}}$$ Hormesis model

$$err(D) = \begin{cases} \beta_1 \times D & \text{for } D < D_{th} \\ \beta_1 \times D_{th} + \beta_2 \times (D - D_{th}) & \text{for } D \geq D_{th} \end{cases}$$ Two-line spline model

$err(D) = \beta_1 \times \exp\{-\beta_2 \exp[-\beta_3 \times (D - D_{th})]\} - \beta_1 \times \exp\{-\beta_2 \exp[-\beta_3 \times (-D_{th})]\}$ Gompertz model

$$err(D) = \begin{cases} 0 & \text{for } D < 0.000001\,\text{Gy} \\ \beta_1 & \text{for } 0.000001 \leq D < 1\,\text{Gy} \\ \beta_2 & \text{for } 1\,\text{Gy} \leq D < 2\,\text{Gy} \\ \beta_3 & \text{for } 2\,\text{Gy} \leq D < 6\,\text{Gy} \\ \beta_4 & \text{for } D \geq 6\,\text{Gy} \end{cases}$$ Categorical model

The hormesis model was introduced by Brain and Cousens (3).

WEB APPENDIX 4: CALCULATION OF AIC-WEIGHTS

For a set of n non-nested models, the AIC-weight, p_m, was calculated for model m according to the following equation (4, 5):

$$p_m = \frac{\exp\left(-\Delta\mathrm{AIC}_m / 2\right)}{\sum_{j=1}^{n} \exp\left(-\Delta\mathrm{AIC}_j / 2\right)} \qquad \text{(A5)}$$

Here, $\Delta\mathrm{AIC}_m = \mathrm{AIC}_m - \mathrm{AIC}_0$, where AIC_m is the AIC-value for model m and AIC_0 is the smallest AIC-value of all n models. The resulting weights, multiplied by a factor of 10^4, give the number of samples for risk estimates to be generated by uncertainty distribution simulations.

In the *sparse model approach*, nested dose-response models with inferior final deviances were eliminated by applying the LRT at a 95% confidence level (details related to this selection process are provided in Web Appendix 6). Subsequently, the criterion for inclusion of a model into the set of final non-nested models, which was used for multi-model inference (MMI), is whether $p_1 > 0.05$ when comparing with the best model, i.e. the one with $\Delta\mathrm{AIC} = 0$ (6, 7). In that case equation (A5) reduces to $p_m = \exp(-\Delta\mathrm{AIC}_m/2)/[\exp(-\Delta\mathrm{AIC}_m/2) + 1]$ with $m = 1$. With this equation it is easy to show that for $\Delta\mathrm{AIC}_1 < 5.9$ one obtains $p_1 > 0.05$. Applying this formula to the four final non-nested models for IHD mortality (Table 2, main text), one finds for the ERR-LNT, ERR-Q and ERR-two-line spline models $p_1 = 0.2503$, $p_1 = 0.4429$, and $p_1 = 0.4101$, respectively (refer to Web Table 3). Consequently, these three models together with the ERR-Gompertz model, which has the smallest AIC-value, survive the selection process. The AIC-weights provided in Table 2 (main text) for the models selected with the sparse model approach were calculated using equation (A5), i.e. they are normalized to 1 to be useful for MMI.

In the *rich model approach*, each model is compared with the best model (i.e. the one with $\Delta\mathrm{AIC} = 0$), applying $p_m = \exp(-\Delta\mathrm{AIC}_m/2)/[\exp(-\Delta\mathrm{AIC}_m/2) + 1]$. Models with $p_1 > 0.05$ survive the selection process (6, 7). The AIC-weights provided in Table 2 (main text) for the models selected with the rich model approach were calculated using equation (A5) because to be useful for MMI they need to sum up to 1.

For all dose-response models that were tested in the present study, the AIC-weights and all related details in the context of the sparse and rich model approaches are provided in Web Table 3.

WEB APPENDIX 5: SOFTWARE

All analyses and model fits that relate to the parametric baseline model (equation (A4)) combined with the dose-response models from Figure 1 and the MMI analyses (sparse and rich model approach) were performed with MECAN (8). It uses Poisson regression to estimate the values of the adjustable model parameters by fitting the model to the grouped CFCS data. For the minimization of the deviance, MECAN applies the MINUIT package for function minimization (9). *ERR* and *EAR* estimates can be calculated directly from h and h_0:

$$ERR = (h/h_0) - 1$$
$$EAR = h - h_0. \quad \text{(A10)}$$

Confidence intervals (CIs) for the *ERR* and *EAR* estimates (both, for the final non-nested models that are included into Occam's group and for MMI) were simulated using multi-variate normal distributions for parameter uncertainties that obey the parameter correlation matrix (10). For a risk variable such as *ERR*, a probability density distribution of 10^4 realizations is generated, which is used to estimate 95% CIs. Central risk estimates were calculated from the MLEs of the model parameters. The MECAN package and all model-related input and result files are available from the authors.

WEB APPENDIX 6: ASPECTS OF MODEL SELECTION ACCORDING TO THE SPARSE MODEL APPROACH

Table 2 provides the main results of fitting the parametric dose-response models from Figure 1 as ERR models to the mortality data for IHD. Considering Figure A1 and applying the LRT four ERR models were identified according to the sparse model approach and were used for MMI. The selection process was performed as follows. The final deviance of the ERR-LNT model (13247.747) was compared with the final deviance of the parametric baseline model (dev = 13252.676). According to the LRT one would argue that adding model parameters β_1 and β_2 (see equation (1) in the main text) to the baseline model did not lead to a significant improvement of the fit at the 5% level because $\Delta dev = 4.93 < 5.99$. When comparing the final deviance of the ERR-Q model with the one of the parametric baseline model one finds $\Delta dev = 6.66$. The problematic of applying the LRT when comparing a baseline model with a dose-response model such as the LNT and Q-models that are multiplied with a dose-effect modifier (11) is, however, known to the authors (in that case the LRT should not be applied because setting parameter $\beta_1 = 0$ also eliminates parameter β_2, which is contained in the DEM). Both models (ERR-LNT and ERR-Q) are included into Occam's group for the following reasons: The ERR-LNT model because, when compared with the best model, it contains an AIC-weight larger than 0.05 (7): According to the formula given in Web Appendix 4 ($p_m = \exp(-\Delta AIC_m/2)/[\exp(-\Delta AIC_m/2) + 1]$) it is easy to see that $p_1 = 0.25$ (see Web Table 3). For the ERR-Q model one finds $p_1 = 0.44 > 0.05$. The ERR-LQ model is nested with the ERR-LNT and ERR-Q models (Figure A1). A comparison of the final deviances between ERR-LQ and ERR-LNT models yields $\Delta dev = 2.36 < 3.84$. Therefore, the additional parameter of the LQ model (β_2) is not statistically significant at the 5% significance level and consequently the ERR-LQ model is not included into the set of final non-nested models used for MMI. Analogous considerations hold for the ERR-LE model, which is nested with the ERR-LNT model: $\Delta dev = 2.07 < 3.84$. For the ERR-LTH model one compares with the ERR-LNT model to find $\Delta dev = 0.93 < 3.84$. Thereby, the ERR-LTH model is not included into the set of final non-nested models either. The smooth step model was implemented as a modified hyperbolic tangent function and is not nested with any of the other dose-response models (Figure A1). Therefore, its final deviance needs to be compared with the one of the baseline model: $\Delta dev = 13252.676 - 13244.451 = 8.22$. Because $8.22 < 9.49$ this model was not included for MMI. The final deviance of the sigmoid model, not nested with any of the models that contain only two or three parameters (Figure A1), was compared with the final deviance of the baseline model to find $\Delta dev = 6.74 < 9.49$. Therefore, the sigmoid model did not survive the selection process as its four parameters were not significant. Although the hormesis model is nested with the sigmoid model, its final deviance needs to be compared with the final deviance of the baseline model because the sigmoid model was not significant. One obtains $\Delta dev = 9.83 < 11.07$. That eliminated the hormesis model. The two-line spline model is nested with the LTH model (Figure A1). The latter was, however, not significant. Consequently, comparison needs to be made with the baseline model and one finds $\Delta dev = 10.39 > 9.49$. Therefore, the ERR-two-line spline model is included into Occam's group. The problematic of applying the LRT in segmented regression (12), as it is the case for the two-line spline model, is known to the authors. Possible related in-depth analyses are, however, out of scope of the present study. The Gompertz model is not nested with any of the applied models. Therefore, its final deviance needs to be compared with the final deviance of the baseline model. It was found that parameter D_{th} was not significant and was therefore set to zero. That reduced the number of

parameters to four (compare with Web Figure 1). Because Δdev = 11.12 > 9.49 the ERR-Gompertz model was included into the set of final non-nested models.

The categorical model with its high number of parameters and biologically implausible shapes does not qualify for MMI. It was applied for a non-parametric characterization of the dose response. It did, however, turn out that the risk prediction for the highest dose category (≥ 6 Gy; *ERR* = 10.26) was accompanied with a very large 95 % confidence interval. Therefore, the risk predictions from the categorical model are not shown in Figures 2 to 4.

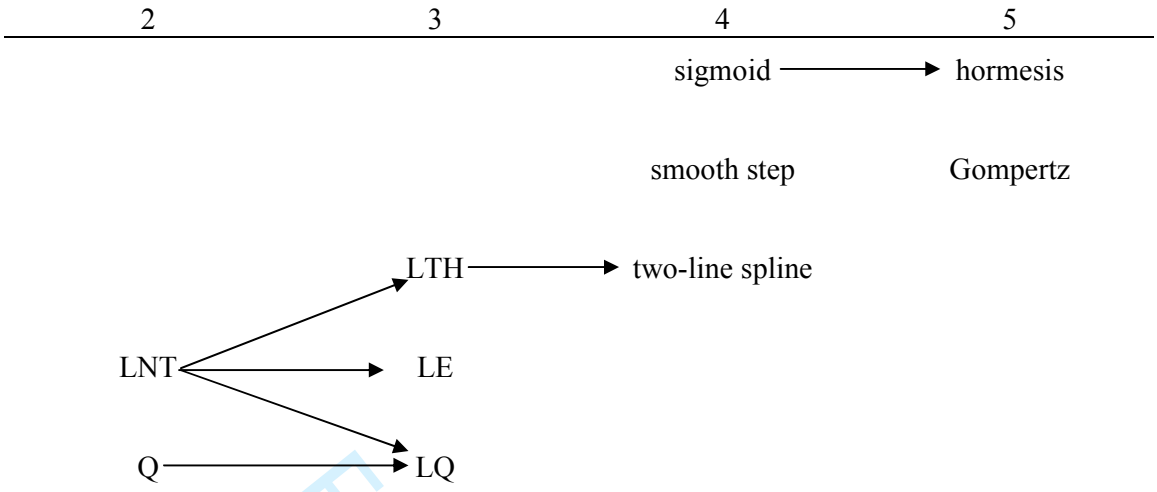

WEB FIGURE 1: Number of model parameters in the dose-response models from Figure 1 and relation between the models (the categorical model is not shown because due to its higher number of model parameters and biologically implausible shapes it is not suited for MMI). Two models are nested if they are connected by an arrow. The smooth step model (modified hyperbolic tangent) and the Gompertz model are not nested with any of the other models. Here, parameter β_2 from equation (A9) was counted as a model parameter for all the dose-response models because all of them contain it within the dose-effect modification.

WEB TABLE 1. Characteristics of the Canadian Fluoroscopy Cohort Study Data (*n*=63707), 1950-1987

Characteristic	No.[c]	Mean	Median	Range
Person-years of follow-up	1902252			
Follow-up, years		31		0-37
Age at end of follow-up, years		65		1-99
Time since first exposure, years		39		0-57
Number of fluoroscopic procedures[a]			64	1-2041
Duration of fluoroscopy screenings, years[a]			2	0-35
Dose fractionation, Gy/year[a]			0.36	0-7.30
Total dose, Gy[b]		0.79		0-11.60

[a] Exposed subjects only.
[b] Cumulative person-time-weighted lung dose.
[c] All values within this table were taken from Table 1 in Zablotska et al. (2).

WEB TABLE 2. Model Parameters, Maximum Likelihood Estimates (MLEs) and Wald-type Standard Errors (in parenthesis) for the Four Final Non-nested Models that were Identified for Occam's group and used for MMI (Sparse Model Approach), Canadian Fluoroscopy Cohort Study, 1950-1987

#	Parameter[a]	ERR-LNT model[b]	ERR-Q model[b]
1	*c_m*	3.485 (0.144)	3.482 (0.144)
2	*c_f*	1.528 (0.208)	1.521 (0.208)
3	*prov_m*	-0.2144 (0.0572)	-0.2138 (0.0571)
4	*prov_f*	-0.1207 (0.0975)	-0.1182 (0.0975)
5	*cdur_m*	-0.00662547	-0.0111411
5	*cdur_f*	-0.00662547	-0.0111411
6	*diag_m*	0.0224 (0.119)	0.0247 (0.119)
7	*diag_f*	0.471 (0.147)	0.476 (0.147)
8	*nostg_m*	0.0951 (0.119)	0.0949 (0.119)
9	*nostg_f*	0.542 (0.140)	0.543 (0.140)
	stg1_m	0	0
	stg1_f	0	0
10	*stg2_m*	0.0217 (0.0444)	0.0284 (0.0443)
11	*stg2_f*	0.1256 (0.0696)	0.1331 (0.0695)
12	*stg3_m*	0.0867 (0.0475)	0.0958 (0.0472)
13	*stg3_f*	0.2937 (0.0742)	0.3028 (0.0740)
14	*ba_m*	5.885 (0.197)	5.879 (0.197)
15	*ba_f*	6.49457 (0.402)	6.492 (0.402)
16	*basq_m*	-4.374 (0.398)	-4.372 (0.398)
17	*basq_f*	-1.669 (0.687)	-1.673 (0.687)
18	*bb_m* (yr^{-1})	-0.1160 (0.0180)	-0.1138 (0.0180)
19	*bb_f* (yr^{-1})	-0.2716 (0.0282)	-0.2689 (0.0281)
20	*bbsq_m* (yr^{-2})	0.03931 (0.00821)	0.03884 (0.00821)
21	*bbsq_f* (yr^{-2})	0.0317 (0.0129)	0.0312 (0.0129)
22		$\beta_1 = 0.1823$ Gy^{-1} (0.0692)	$\beta_1 = 0.1420$ Gy^{-2} (0.0474)
23		$\beta_2 = -12.01$ yr Gy^{-1} (3.39)	$\beta_2 = -14.57$ yr Gy^{-1} (3.86)
	dev	13247.75	13246.01

#	Parameter[a]	ERR-two-line spline model[c]	ERR-Gompertz model[d,e,f]
1	*c_m*	3.449 (0.145)	3.479 (0.145)
2	*c_f*	1.493 (0.208)	1.507 (0.208)
3	*prov_m*	-0.2165 (0.0572)	-0.2180 (0.0572)
4	*prov_f*	-0.1192 (0.0976)	-0.1127 (0.0975)
5	*cdur_m*	-0.0409877	-0.0208749
5	*cdur_f*	-0.0409877	-0.0208749
6	*diag_m*	0.029 (0.120)	0.0232 (0.119)
7	*diag_f*	0.476 (0.147)	0.482 (0.147)
8	*nostg_m*	0.097 (0.119)	0.0930 (0.119)
9	*nostg_f*	0.541 (0.140)	0.544 (0.140)
	stg1_m	0	0
	stg1_f	0	0
10	*stg2_m*	0.0290 (0.0446)	0.0270 (0.0447)
11	*stg2_f*	0.1306 (0.0697)	0.1440 (0.0695)
12	*stg3_m*	0.0922 (0.0478)	0.0903 (0.0484)
13	*stg3_f*	0.2956 (0.0744)	0.3227 (0.0739)
14	*ba_m*	5.882 (0.198)	5.871 (0.198)
15	*ba_f*	6.489 (0.402)	6.499 (0.402)
16	*basq_m*	-4.371 (0.399)	-4.357 (0.399)
17	*basq_f*	-1.661 (0.687)	-1.695 (0.687)
18	*bb_m* (yr^{-1})	-0.1132 (0.0182)	-0.1152 (0.0182)
19	*bb_f* (yr^{-1})	-0.2693 (0.0282)	-0.2654 (0.0281)
20	*bbsq_m* (yr^{-2})	0.03934 (0.00822)	0.03914 (0.00824)
21	*bbsq_f* (yr^{-2})	0.0319 (0.0129)	0.0305 (0.0129)
22		β_1 = 0.3571 Gy^{-1} (0.0922)	β_1 = 6.48 (9.82)
23		β_2 = 2.006 Gy^{-1} (0.755)	β_2 = 7.28 (2.11)
24		D_{th} = 1.7246 Gy (0.0649)	β_3 = 0.684 Gy^{-1} (3.49)
25		β_3 = -9.32 yr Gy^{-1} (1.85)	β_4 = -10.60 yr Gy^{-1} (2.86)
			D_{th} = 0
		13242.28	13241.55

Abbreviations: dev, final deviance; ERR-LNT, linear no-threshold implemented as excess relative risk model; ERR-Q, quadratic model implemented as excess relative risk model.

[a] Parameters 1 to 21 are the baseline parameters, parameters 22 to 25 are the radiation-associated parameters.

[b] For the ERR-LNT and ERR-Q models parameter β_2 is related to the adjustment for dose-fractionation modifications (see equation (1) in the main text).

[c] For the ERR-two-line spline model the adjustment for dose-fractionation is associated with parameter β_3.

[d] For the ERR-Gompertz model the adjustment for dose-fractionation is associated with parameter β_4.

[e] It was found that for the fit of the Gompertz model the parameter D_{th} was not significantly different from zero. Therefore, D_{th} was fixed at zero. Consequently, this model has four radiation-associated model parameters (compare with Web Figure 1 where the five listed parameters still include D_{th}).

[f] It is noted that for the error calculations related to Figures 2 to 4 two of the dose-response parameters of the Gompertz model (β_2 and β_3) were fixed at their MLEs. Otherwise the 95% CIs of the model-related risk predictions and in consequence the MMI-related 95% CIs would turn out as too large.

WEB TABLE 3. Results of Fitting the Dose-Response Models From Figure 1 as ERR Models to the Mortality Data for IHD including the two different types of AIC-weights, Canadian Fluoroscopy Cohort Study, 1950-1987 (2)

Sparse model approach								
Model	**dev**	**Δdev[a]**	**N_{par}**	**AIC[b]**	**ΔAIC[c]**	**Normalized AIC-weights[d]**	**Bilateral AIC-weights[e]**	**Rounded nsim[f]**
ERR-LNT	13247.75	6.19	23	13293.75	2.19	0.1183	0.2503	2303
ERR-Q	13246.01	4.46	23	13292.01	0.46	0.2815	0.4429	4513
ERR-two line spline, D_{th} = 1.72 Gy	13242.28	0.73	25	13292.28	0.73	0.2461		4513
ERR-Gompertz, D_{th} = 0	13241.55	0	25	13291.55	0	0.3541	0.4101	3184
Rich model approach[g]								
Model	**dev**	**Δdev**	**N_{par}**	**AIC**	**ΔAIC**	**Normalized AIC-weights**	**Bilateral AIC-weights**	**Rounded nsim**
ERR-LNT	13247.75	6.19	23	13293.75	2.19	0.0776	0.2503	776
ERR-Q	13246.01	4.46	23	13292.01	0.46	0.1847	0.4429	1847
ERR-LQ	13245.38	3.83	24	13293.38	1.83	0.0930	0.2859	930
ERR-LE	13245.68	4.13	24	13293.68	2.13	0.0802	0.2566	802
ERR-LTH, D_{th} = 0.58 Gy	13246.81	5.26	24	13294.81	3.26	0.0455	0.1639	455
ERR-smooth step, D_{th} = 4,47 Gy	13244.45	2.90	25	13294.45	2.90	0.0546	0.1902	546
ERR-sigmoid, D_{th} = 41,53 Gy	13245.94	4.39	25	13295.94	4.39	0.0259	0.1004	259
ERR-hormesis, D_{th} = 3,28 Gy	13242.84	1.29	26	13294.84	3.29	0.0449	0.1620	449
ERR-two-line spline, D_{th} = 1.72 Gy	13242.28	0.73	25	13292.28	0.73	0.1615	0.4101	1615
ERR-Gompertz, D_{th} = 0	13241.55	0	25	13291.55	0	0.2323		2323
ERR-categorical	13242.19	0.63	29	13300.19	8.63		0.0132	
Baseline	13252.68		21	13294.68				

Abbreviations: AIC, Akaike Information Criterion; dev, final deviance; nsim, number of samples for risk estimates to be generated by uncertainty distribution simulations; ERR-LNT, linear no-threshold model implemented as excess relative risk model; ERR-Q, quadratic model

implemented as excess relative risk model; ERR-LQ, linear-quadratic model implemented as excess relative risk model; ERR-LE, linear-exponential model implemented as excess relative risk model; ERR-LTH, linear threshold model implemented as excess relative risk model.

[a] The difference in final deviance is denoted by Δdev with respect to the model with the smallest final deviance.

[b] AIC = dev + 2 × N_{par}, where N_{par} is the number of model parameters.

[c] The difference in AIC-values with respect to the model with the smallest AIC-values is denoted by ΔAIC.

[d] The normalized AIC-weights were calculated with equation (A5) from Web Appendix 4.

[e] For the bilateral AIC-weights one model at a time is compared to the best model, i.e. the one with ΔAIC = 0, so that equation (A5) reduces to the following equation: $p_m = \exp(-\Delta AIC_m/2)/[\exp(-\Delta AIC_m/2) + 1]$ with $m = 1$ (refer to Web Appendix 4). Except for the ERR-categorical model, all bilateral AIC weights of both the rich and the sparse model approaches exceed 0.05. Thus, all corresponding models are eligible for MMI.

[f] The normalized AIC-weights, multiplied by a factor of 10^4, give the number of samples (nsim) for risk estimates to be generated by uncertainty distribution simulations.

[g] For the error calculations within the rich model approach some of the dose-response parameters of 5 out of the 10 surviving models were fixed at their MLEs. Otherwise the 95% CIs of the model-related risk predictions would turn out as too large.

REFERENCES

1. Simonetto C, Azizova TV, Grigoryeva ES, et al. Ischemic heart disease in workers at Mayak PA: Latency of incidence risk after radiation exposure. *PLOS ONE*. 2014;9(5):e96309.

2. Zablotska LB, Little MP, Cornett RJ. Potential increased risk of ischemic heart disease mortality with significant dose fractionation in the Canadian Fluoroscopy Cohort Study. *Am J Epidemiol*. 2014;179(1):120-131.

3. Brain P, Cousens R. An equation to describe dose responses where there is stimulation of growth at low doses. *Weed Res.* 1989;29:93–96.

4. Burnham KP, Anderson DR. *Model selection and multimodel inference*. 2nd ed. New York: Springer; 2002.

5. Claeskens G, Hjort NL. Model selection and model averaging. Cambridge: Cambridge University Press; 2008.

6. Hoeting JA, Madigan D, Raftery AE, et al. Bayesian model averaging: a tutorial. *Statist Sci*. 1999;14(4):382–417.

7. Walsh L. A short review of model selection techniques for radiation epidemiology. *Radiat Environ Biophys*. 2007;46(3):205-213.

8. Kaiser JC. MECAN. A software package to estimate health risks in radiation epidemiology with multi-model inference. User Manual. Version 0.2 (Helmholtz Zentrum München, Neuherberg, Germany). 2010.

9. Moneta L, James F. Minuit2 minimization package. http://seal.web.cern.ch/seal/snapshot/work-packages/mathlibs/minuit, April 2010. v. 5.27.02.

10. Kaiser JC, Walsh L. Independent analysis of the radiation risk for leukaemia in children and adults with mortality data (1950-2003) of Japanese A-bomb survivors. *Radiat Environ Biophys*. 2013;52(1):17-27.

11. Liu X, Shao Y. Asymptotics for likelihood ratio tests under loss of identifiability. *The Annals of Statistics*. 2003;31(3): 807–832.

12. Feder PI. The log likelihood ratio in segmented regression. *The Annals of Statistics*. 1975; 3(1):84-97.